A 96-well Format Microvascularized Human Lung-on-a-Chip Platform for Microphysiological Modeling of Fibrotic Diseases

SCHOLARONE™
Manuscripts

1   **Title:** A 96-well Format Microvascularized Human Lung-on-a-Chip Platform for

2   Microphysiological Modeling of Fibrotic Diseases

3

4   **Authors:** Joscelyn C. Mejías, Michael R. Nelson, Olivia Liseth, Krishnendu Roy*

5

6   **Affiliation:** Wallace H. Coulter Department of Biomedical Engineering at Georgia Tech and

7   Emory, Marcus Center for Therapeutic Cell Characterization and Manufacturing, NSF ERC for

8   Cell Manufacturing Technologies (CMaT), The Georgia Institute of Technology

9

10

11   **Corresponding Author:**

12   Krishnendu Roy, PhD

13   Robert A. Milton Chair Professor

14   Director, Center for ImmunoEngineering

15   Director, NSF ERC for Cell Manufacturing Technologies (CMaT)

16   Director, Marcus Center for Therapeutic Cell Characterization and Manufacturing (MC3M)

17   The Wallace H. Coulter Department of Biomedical Engineering at Georgia Tech and Emory

18   Georgia Institute of Technology

19   EBB 3018, 950 Atlantic Dr., Atlanta, GA 30332, USA

20   Phone: (404) 385 6166; E-mail: krish.roy@gatech.edu

21

22 **Abstract**

23 Development of organoids and microfluidic on-chip models have enabled studies of organ-level

24 disease pathophysiologies *in vitro*. However, current lung-on-a-chip platforms are primarily

25 monolayer epithelial-endothelial co-cultures, separated by a thin membrane, lacking

26 microvasculature-networks or interstitial-fibroblasts. Here we report the design,

27 microfabrication, and characterization of a unique microphysiological on-chip device that

28 recapitulates the human lung interstitium-airway interface through a 3D vascular network, and

29 normal or diseased fibroblasts encapsulated within a fibrin-collagen hydrogel underneath an

30 airlifted airway epithelium. By incorporating fibroblasts from donors with idiopathic pulmonary

31 fibrosis (IPF), or healthy-donor fibroblasts treated with TGF-β1, we successfully created a

32 fibrotic, alpha smooth muscle actin (αSMA)-positive disease phenotype which led to fibrosis-

33 like transformation in club cells and ciliated cells in the airway. Using this device platform, we

34 further modeled the cystic fibrosis (CF) epithelium and recruitment of neutrophils to the vascular

35 networks. Our results suggest that this microphysiological model of the human lung could enable

36 more pathophysiologically relevant studies of complex pulmonary diseases.

37

38   **Graphical Abstract**

39
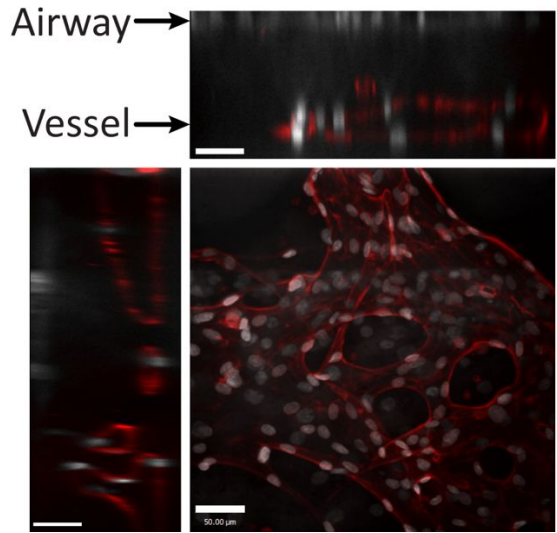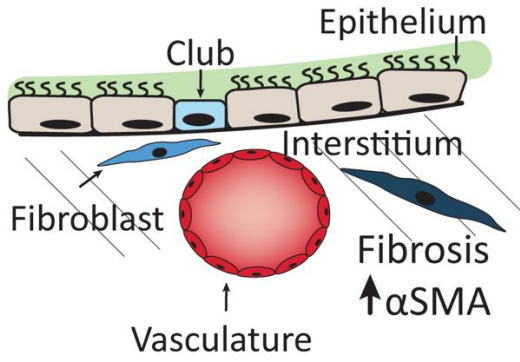
40

41

42   **Introduction**

43   The respiratory airways are a complex network of pseudostratified epithelium separated

44   from blood vessels by a thin basement membrane. Each of these components is critical to

45   maintaining normal lung physiology and is affected by diseased states such as chronic

46   obstructive pulmonary disease (COPD), asthma, idiopathic pulmonary fibrosis (iPF), and cystic

47   fibrosis (CF). Recent airway-on-a-chip microfluidic devices composed of a pseudostratified

48   epithelium separated from a single layer endothelium by a synthetic porous membrane have

49   allowed for simplified aspects of the lung environment to be recreated to study the biochemical

50   and metabolic activity in normal and diseased states[1]. 3D printed macroscale models have been

51   shown to form vascular network below a transwell-based epithelium, however, current models

52   lack fibroblasts necessary to recapitulate fibrotic airways[2]. Additional lung-on-a-chip models,

53   have included a third layer of the single microfluidic channel to incorporate fibroblasts and

54   lamina propria between the epithelium and endothelial layers[3,4]. While these models allow for

55   easier platforms to study pulmonary diseases, they lack important aspects of the airway 3D

56   microenvironment, specifically the underlying interstitial space and vasculature network.

57   3D perfusable microvasculature organs-on-a-chip have been developed to study normal

58   and diseased vascular states with incorporation of neutrophil or cancer extravasation[5,6]. Oh et al

59   expanded this model to include a secondary large porous poly(dimethylsiloxane) (PDMS) layer

60   to study cancer spheroid-vasculature interaction and recently Paek et al developed an open-top

61   microvascular device to replicate the blood-retinal barrier[7,8]. Here, we adapt the microvascular 5-

62   channel microfluidic devices to create a multi-layer microphysiologic device to produce an air-

63   liquid interface (ALI) of the upper respiratory airways above a perfusable vascularized

64   endothelial network with healthy/diseased fibroblasts within a hydrogel matrix. We successfully

65   fabricated this device with the standard 0.4 µm polyester track-etched (PETE) porous membrane

66   and expand the design to include a more physiologically relevant native extracellular matrix

67   (ECM)—a vitrified collagen thin film[9]. We incorporated this microvascular multi-layer

68   interstitium-airway model into a high-throughput 96-well platform for easier fabrication,

69   handling, and integration with automated imaging platforms. We confirmed successful ALI

70   epithelial differentiation with beta-tubulin 4 (Tubb4) and ZO-1 formation in the epithelium

71   above these networks. We used this microvascularized epithelium to create both induced and iPF

72   derived fibrosis models with increased αSMA expression and observed changes in both club cell

73   uteroglobin (CC10) and Tubb4 expression in the airway epithelium. We further expanded this

74   platform to other diseases such as cancer and CF with the incorporation of neutrophils. We

75   believe this model recapitulates key aspects of the 3D lung microenvironment for studying

76   fibroblast-endothelium-epithelium interactions that are currently missing in current lung-on-a-

77   chip or lung organoid models.

78

79   **Materials and Methods**

80   _Device Fabrication:_ The macrophysiologic device was designed in four parts: (A)

81   photolithography based vascular layer, (B) 3D printed airway layer, (C) polyester track etched

82   (PETE) or vitrified collagen membranes, and (D) a commercially available bottomless 96-well

83   plate (Greiner Bio-One, Monroe USA). The vascular layer was fabricated based on previous

84   microvasculature designs[6] with minor modifications described in Nelson et al.[10] on a silicon

85   wafer using SU-8 2150 (MicroChem Corp., Westborough USA) using standard photolithography

86   techniques. The silicon master with a 2 x 2 array was poured using 10:1 base:curing agent PDMS

87   (Ellsworth Adhesives, Germantown USA). Two vascular layers were used per 96-well plate.

88   Airway masters were printed in Systems Accura 60 (Protolabs, Maple Plain USA) with a

89   2 x 4 array of a 1 x 1 x 9 mm central channel aligned to match directly over the vascular layer

90   central channel and 1 mm guide marks matching the vascular layer ports, Fig S1. Airways were

91   poured using a 10:1 base:curing agent PDMS. For each device in the 2 x 4 array, a 1 mm biopsy

92   punch (Miltex, York USA) was used to punch 10 of the ports; a 2 mm punch (Miltex) was used

93   for the final two ports—one port of each media channel to reduce bubbles during media

94   exchanging, Fig 1B.

95   The punched airway layer was then bonded to the bottomless 96-well plate as previously

96   described[11]. Briefly, bottomless 96-well plates were immersed in a 2% v/v solution of 3-

97   mercaptopropyl timethoxysilane (Sigma Aldrich, St. Louis USA) diluted in methanol (VWR

98   BDH Chemicals, Radnor USA) for 1 minute, rinsed with deionized water, and air dried. Plates

99   and PDMS airway layers were plasma treated with a Harrick Plasma Cleaner (PDC-001, Ithaca

100   USA), aligned, bonded together with airway features facing away from the plate, and left at 65°C

101   overnight.

102   Plates were fabricated with either PETE or collagen membranes. PETE membranes were

103   bonded over each airway channel with (3-aminopropyl)triethoxysilane (APTES) as previously

104   described[12]. Briefly, optically transparent 0.4 μm PETE membranes were cut from 6-well

105   Transwells (Corning Inc., Corning USA), plasma treated for 20 seconds, and placed in 5%

106   APTES preheated to 80°C for 10 minutes. Membranes were then dried on a Kimwipe, the 96-

107   well plate-airway and vasculature PDMS layer surfaces was then immediately activated with

108   oxygen plasma and the membrane was sandwiched between the two PDMS pieces. Coverslips

109   were then bonded to the bottom of each device of the final 96-well plate. 24 hours before use to

110   improve cell adherence to the PETE membrane, the membrane was collagen coated with the

111   assist of dopamine as previously described[10,13]. Briefly, 15 μl of freshly made 0.01 % wt/vol

112   dopamine hydrochloride (Sigma Aldrich) in 10 mM Tris HCl, pH 8.5 was added to each airway

113   channel. After 1h at room temperature airways were washed with PBS, all fluid was aspirated,

114   and 15 μl of 20 μg/mL rat tail collagen I was added to each airway channel. After incubating for

115   1h at room temperature the airway channels were rinsed with PBS and allowed to completely dry

116   before the plate was UV sterilized.

117   Vitrified collagen membranes were made, as previously described[9,14], directly on the

118   punched airway channel (bonded to 96 well plate) by mixing rat tail type 1 high concentrated

119   collagen (Corning) with 10x PBS, 1N NaOH, DI water following manufacturer's instructions for

120   a final collagen concentration of 4 mg/mL. Once well mixed approximately 40-55 μL of collagen

121   was pipette across the open airway channel, incubated in a 37°C humid incubator for 45-60

122   minutes, then allowed to dry at room temperature overnight. The hydrophobicity of PDMS will

123   keep the collagen out of the channel, if the collagen is pipetted into the channel the device should

124   not be used. Membranes were then rinsed with DI water for 5 minutes, water was aspirated

125   without touching the membrane, and membranes were left to dry. Once dried the vascular layers

126   were bonded with oxygen plasma to the 96-well plate-airway. Coverslips were then bonded to

127   the bottom of each device of the final 96-well plate. Plates were UV sterilized for 2h before use.

128   *Cell Culture and Seeding:* Cell catalog and lot information can be found in Table S1.

129   Normal Human Lung Fibroblasts (NHLF, Lonza, Walkersville USA) and Idiopathic Pulmonary

130   Fibrosis Human Lung Fibroblasts (iPF-HLF, Lonza) were grown to passage 7 in Fibroblast

131   Growth Medium-2 BulletKit (Lonza). Human Umbilical Vein Endothelial Cells (HUVECs,

132   Lonza) were grown on 0.1% Bovine Gelatin (Sigma Aldrich) coated flasks up to passage 8 in

133   Microvascular Endothelial Cell Growth Media-2 BulletKit (EGM2MV, Lonza). Normal Human

134   Small Airway Epithelial Cells S-ALI Guaranteed (SAECs, Lonza) were grown in PneumaCult-

135   Ex Plus (Stemcell Technologies, Vancouver Canada) to passage 3 and differentiated in

136   PneumaCult-ALI medium (Stemcell Technologies, Vancouver Canada). Endothelial cells with

137   iPF-HLF or NHLF were resuspended in human thrombin (4 U/mL, Sigma Aldrich) mixed 1:1

138   with a 9/1 mg/mL human fibrinogen (Sigma Aldrich)- rat tail type 1 high concentrated collagen

139   mixture (ThermoFisher Sci., Waltham USA), and flowed into the lower central channel for a

140   final concentration of HUVECs at 6×10^6 cells/mL and iPF-HLF at 0.3×10^6 cells/mL. NHLF

141   were resuspended in thrombin at 6×10^6 cells/mL (4 U/mL) mixed 1:1 with a 10/0.1 mg/mL

142   fibrinogen (Sigma Aldrich)/PEG-disuccinimidyl valerate (SVA-PEG-SVA, 3400 Da, Laysan

143   Bio, Arab USA) and flowed into the outer two side channels. SVA-PEG-SVA was added to the

144   outer fibrin channels after repeated cultures showed that after 5 days of cultures the NHLFs

145   contracted the gels off the ports. After seeding all 8 devices, the 96-well plates were then placed

146   in a 37°C humid incubator to gel for 15 minutes before the addition of EGM2MV supplemented

147   with 50 ng/mL human VEGF (PeproTech, Rocky Hill USA) into the media reservoirs (including

148   into the non-seeded airway channel), media was then moved daily and exchanged every even

149   day. On Day 2 hSAECs were seeded in the top airway channel at 2.5×10^6 cells/mL in

150   PneumaCult-Ex Plus; vasculature media was exchanged for EGM2MV supplemented with 50

151   ng/mL VEGF and 100 ng/mL human Angiopoietin-1 (PeproTech). SAECs were airlifted by

152   pipetting the media out of the upper channel on Day 4. Once airlifted, a 50/50 mixture of

153   EGM2MV/PneumaCult-ALI was used to feed the device until the end of cultures. TGF-β1

154   (PeproTech) and Pirfenidone (Cayman Chemical, Ann Arbor USA) were later added by diluting

155   frozen stock solutions prepared and stored at -80°C according to manufacturer's instructions.

156   For vitrified collagen devices bovine fibrinogen (Sigma Aldrich) and rat tail type 1 high

157   concentrated collagen were mixed at 8/1 mg/mL before mixing with HUVECs/HLFs in human

158   thrombin. Neutrophils (Astarte, Bothell USA) were stained with CellTracker Deep Red, see

159   supplemental methods, and added at 5×10^5 to one media port of each device. LTB4 (100

160   ng/mL, Cayman Chemicals), LPS (0.1 mg/mL, Sigma Aldrich), or PBS were added to the airway

161   channels and devices were incubated for 3 hours before perfusion and fixation.

162   *Perfusion*: Device perfusion was imaged using a BioTek Lionheart system with a 4x

163   objective. Montage parameters were set on each individual device, 50 µL of 10 µg/mL 70 kDa

164   FITC-dextran in PBS was added to one media port and the plate was immediately imaged.

165   Images were stitched and contrasted with Gen5 v. 3.04. For the percentage of perfusable area

166   analysis the stitched images were straightened and cropped to remove the ports using Adobe

167   Photoshop. Cropped images were then analyzed for fluorescent area using FIJI[15] by adjusting the

168   threshold until all vessels were captured. For the neutrophil imaging, after fixation and staining,

169   devices were imaged by autofocusing on the CellTracker Deep Red labeled neutrophils across

170   the entire central channel. Images were than stitched and Gen5 was used to calculate the area of

171   fluorescent neutrophils.

172   **Immunostaining**

173   Devices were stained as previously described[5] with antibodies listed in Table S2. Briefly,

174   devices were washed 3 x with 200 µl PBS per media port, fixed with 4% paraformaldehyde

175   (ThermoFisher) for 10 minutes, permeabilized for 15 minutes with 0.1% v/v Triton X-100

176   (Sigma Aldrich), washed with PBS, and then blocked for 3 hours at room temperature with 5%

177   w/v BSA (Sigma Aldrich) and 4% v/v goat serum (ThermoFisher). Primary antibody was diluted

178   1:100 in the blocking buffer and devices were stained overnight at 4°C. Devices were then

179   washed with 0.1% w/v BSA in PBS. Devices were incubated with secondary antibodies diluted

180   at 1:250 and DAPI (Sigma Aldrich) diluted to 1:1000 in blocking buffer for 3 hours at room

181   temperature. For devices stained with CD31 and a primary needing a secondary mouse,

182   primary/secondary staining was done first followed by CD31 staining overnight at 4°C. To

183   reduce CC10 and Tubb4 waste, Tubb4 and corresponding secondary were added to the airway

184   channel only. Devices were then washed in 0.1% BSA and imaged.

185   *Confocal Microscopy*: Fluorescent images were collected on a PerkinElmer UltraVIEW

186   VoX spinning disk confocal microscope with a Hamamatsu C9100-23b back-thinned EM-CCD

187   and Nikon 10x NA-0.3 air objective, Nikon S Plan Fluor ELWD (extra-long working distance)

188   20x NA-0.45 air objective, or Nikon S Plan Fluor ELWD 60x NA-0.70 air objective. To account

189   for variability in the laser over time, devices for each experiment were imaged in a single session

190   and devices from experimental groups were randomized during the session. Each device was

191   imaged in 4-6 regions in the central channel. Fluorescent area percentages were measured

192   relative to the total area of each image using Volocity software (Perkin Elmer Inc., Waltham

193   USA) with the fluorescence threshold set using control devices stained with the isotype or

194   secondary only (no primary).

195   *Statistical Analysis*: Data were analyzed in GraphPad Prism. Data normality was assessed using

196   the Shapiro-Wilk test ($\alpha = 0.05$). A two-way ANOVA ($\alpha = 0.05$) with post-hoc Tukey's test with

197   adjusted P value for multiple comparisons was used for analyses of significance. The fibrosis

198   experiments, Figs. 2 and 3, yielded non-normal distributions (Shapiro Wilk), therefore statistical

199   significance data should be interpreted with caution.

200

201   **Results & Discussion**

202   The microphysiologic device was designed to replicate key features of the lower

203   respiratory airways, specifically the blood vessel-interstitium fibroblast-epithelial

204   microenvironment, schematic Fig. 1A. To accomplish this, a multi-layer device was made from a

205   bottomless 96-well plate and two PDMS layers; each PDMS layer was individually fabricated

206   before all three pieces were irreversibly bonded together. To recreate the vascular networks a

207   previously described 5-channel device was utilized[6,10]. The two outer channels were seeded with

208   Normal Human Lung Fibroblasts (NHLF) in a fibrin gel. These cells provide cytokine gradients

209   to direct vasculogenesis of the HUVEC/HLF (HUVEC: Human Umbilical Vein-derived

210   Endothelial Cells) fibrin gel culture in the central channel. The second PDMS layer was designed

211   for a single airway channel to sit directly above this central HUVEC/HLF channel for epithelial

212   cell growth; this PDMS layer also provided the open ports to seed and feed both culture layers,

213   PDMS layer overview Fig. 1B. A 0.4 μm PETE or collagen membrane was sandwiched between

214   the two PDMS layer feature sides to allow for gel loading and epithelial cell support, device

215   cross section view Fig. 1C. This 3D design is unique as it allows for culture of epithelium

216   directly above a vascular network of endothelium and fibroblasts.

217   The bottomless 96-well plate was utilized to provide the media reservoirs for the

218   microphysiologic devices. A 2 x 4 array of these devices was aligned to the 96-well plate format

219   (an exploded device view is shown in Fig. 1D). While individual stand-alone devices can be

220   fabricated, the chemical bonding to a 96-well plate increased the surface area of the PDMS

221   around the device, reducing leaking while also providing physical support to prevent human

222   error in handling the devices such as deforming the device and causing the membrane to separate

223   from the PDMS. This format also allowed for larger batch fabrication and integration with

224   automated plate systems. The microvasculature portion of the device was seeded first; attempts

225   at first differentiating epithelium introduced too much humidity in the lower portion of the

226   device to allow for successful gel loading. After the microvasculature sprouting, Small Airway

227   Epithelial Cells (SAECs) were seeded. The SAECs were then transitioned to an air-liquid

228   interface on the next even day of culture, media was exchanged for a 50:50

229   EGM2MV/PneumaCult ALI mixture until the end of the co-culture experiment (see growth

230   schematic, Fig. 1E).
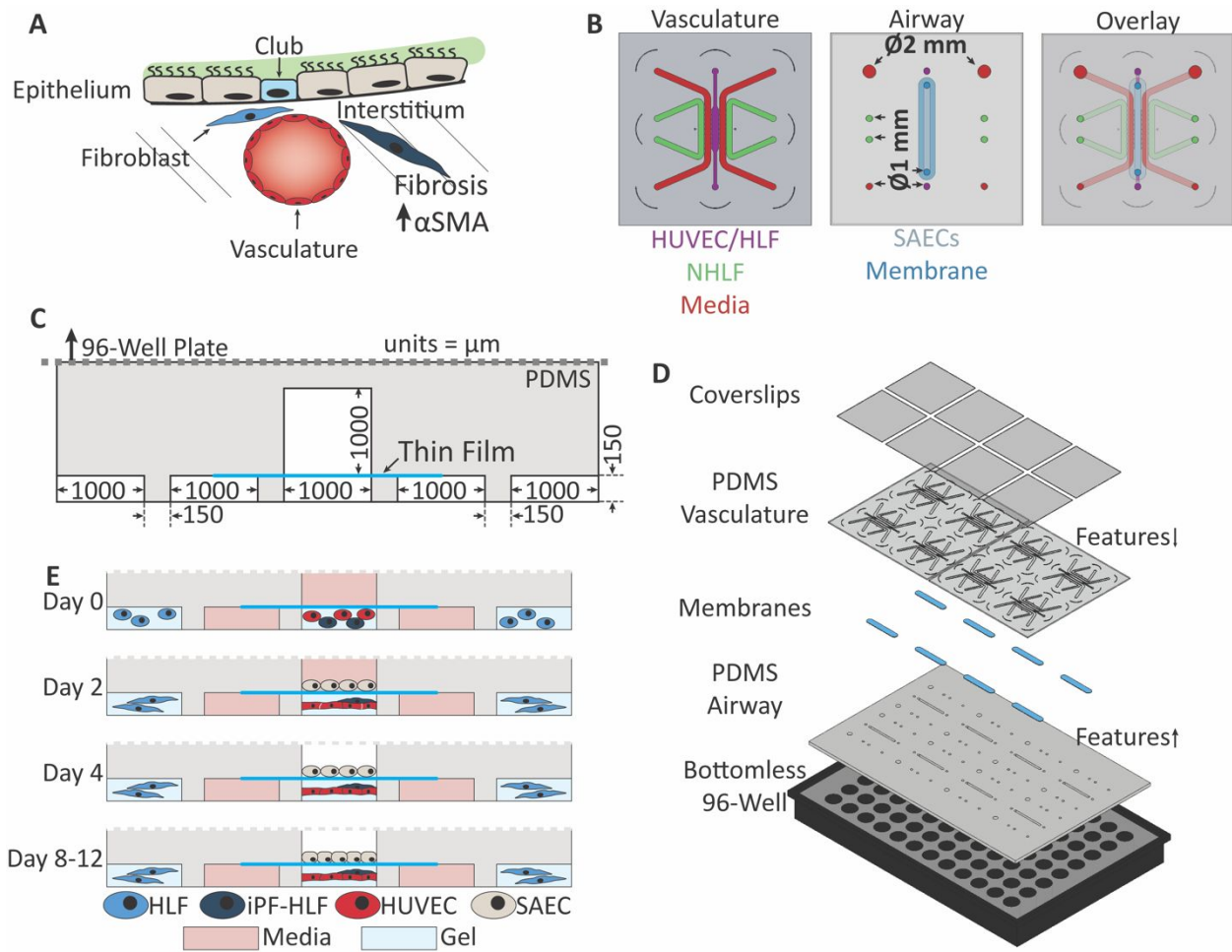
232   ***Fig. 1. Device and 96-well plate conceptual overview*** *(A) Schematic representation of*

233   *tissue recapitulated within the device (B) Single device PDMS layer diagrams. (C) Cross-section*

234   *schematic of a single device. (D) Exploded view of the full 96-well format. (E) Cell seeding and*

235   *growth schematic*

236

237   Initial devices suffered from poorly perfusable microvasculature due to a lack of open

238   ports along the central channel. To improve this, fibroblast donor lot screening of 5 available lots

239   of NHLF was done with simple vascular devices to select for the lot with the most consistent

240   open ports and therefore perfusable networks, supplemental methods, Table S1, Fig. S2. The lot

241   defined as NHLF-A was found to reproducibly create 100% of devices with at least one set of

242   open, perfusable ports. Interestingly, this donor was defined as a smoker. NHLF-A was chosen

243   for the outer channels and varying lots (defined in each experiment) were co-cultured with

244   HUVECs in the central channel. SAECs were then seeded/airlifted in the upper airway channel.

245   To improve the perfusable area of the central channel and the percentage of open ports, vascular

246   endothelial growth factor (VEGF) and Angiopoietin-1 (Ang-1) were added to the media for the

247   first four days of culture (D0-D2 VEGF, D2-D4 VEGF/Ang1). With this setup PETE-based

248   normal "healthy" devices all had at least 50% of the ports open and 92% of all devices (with and

249   without treatment and diseased donors) had over 50% of their ports open.

250   This device design allowed for the use of either PETE or vitrified-collagen based

251   membranes to separate the epithelium from the vasculature. PETE or collagen devices were

252   seeded with NHLF-A/HUVEC co-cultures for the vasculature and SAECs for the epithelium

253   grown at an air-liquid interface for 5 days. Extended focus Z-stacks of the epithelium taken using

254   a 20x ELWD lens show expected tight junction formation (ZO-1), Figure 2A, due to high

255   autofluorescence of the PETE membrane images were linearly contrasted separately. To test that

256   vasculature formation held with co-cultures of HUVECs with other fibroblast lots in the central

257   channel, healthy (NHLF-B) or diseased (iPF-HLF) fibroblasts were co-cultured below SAECs

258   and after 9 days of culture perfused and fixed/stained. Perfusion with 70 kDa FITC-dextran

259   showed vascular network formation with both fibroblast lots, Figure 2B, while nuclei (DAPI –

260   white) and endothelial (CD31 – red) staining confirmed the 3D vascular network below the

261   airway epithelium, representative NHLF-B shown in Figure 2C.

262
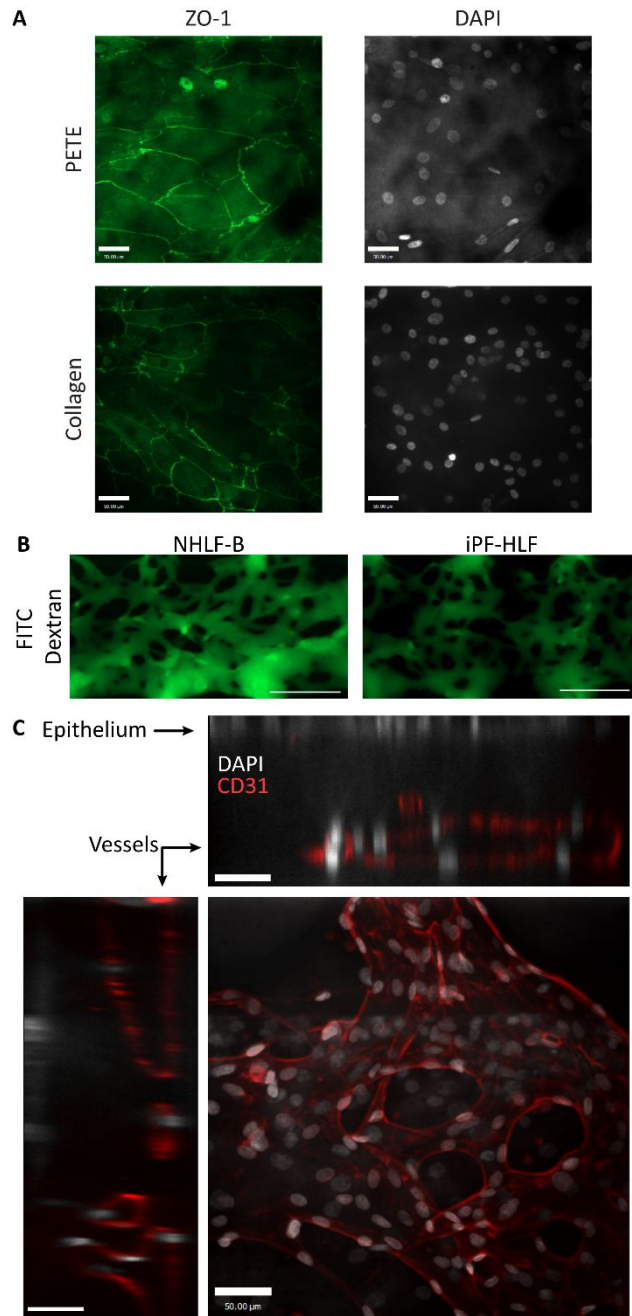
263   *Fig. 2. Characterization of the 3D Microvascular Network and Airway Epithelium*

264   *of Lung-on-Chip Devices. The lower compartment (mimicking the interstitial tissue) of the*

265   *microphysiologic devices were seeded with HUVECs and either healthy (NHLF) or diseased*

266   *(iPF-HLF) human donor or patient-derived fibroblasts. The upper compartment (airway*

267   *epithelium) was seeded with SAECs on PETE or collagen membranes. (A) Extended focus z-*

268   *stack of Nuclei (DAPI – white) and tight junctions (ZO-1, green) staining of airway epithelium*

269   *on PETE or Collagen membranes, scale bar = 50 μm (B) 70 kDa FITC-Dextran is perfusable*

270   *through the microvascular network formed in both healthy (NHLF-B) and diseased (iPF-HLF)*

271   *fibroblast containing devices, scale bar = 500 μm (C) Extended focus image of representative*

272   *NHLF-B vasculature nuclei (white-DAPI) and endothelium (red-CD31) with XY, XZ, and YZ side*

273   *views showing vessels below the epithelial layer nuclei, scale bar = 50 μm. All images were*

274   *linearly contrasted to enhance clarity.*

275

276   Idiopathic pulmonary fibrosis (iPF) is a pulmonary disorder marked by increased

277   fibrosis—excessive accumulation of extracellular matrix proteins (e.g. collagens) and activated

278   fibroblasts within the interstitium. Once believed to be an inflammatory disease it is now

279   believed to be driven by epithelial-fibroblast crosstalk[16,17]. TGF-β1 has been previously shown

280   to be a key driver in pulmonary fibrosis and has been used in many organoid *in vitro* cultures to

281   push fibroblasts toward a more myofibroblast phenotype with increased αSMA production[18–21].

282   To create a fibrosis model in our lung-on-a-chip we took two approaches: (a) seed primary donor

283   iPF patient derived-diseased human iPF-HLFs alongside the HUVECs and/or (b) induce a more

284   myofibroblast phenotype in the device (i.e. increased αSMA) with TGF-β1 treatment of healthy

285   (NHLF) or diseased iPF-HLF co-culture. Microphysiologic 96-well plates fabricated with 0.4

286   μm PETE membranes were seeded with two different lots of NHLFs (NHLF-A, NHLF-B) or

287   iPF-HLF in the central channel alongside HUVECs. For all devices NHLF-A was used to seed

288   all outer channels. We cultured the seeded devices normally up to Day 6 before adding 5 or 10

289   ng/mL of TGF-β1 into the media for 3 days. At the end of the culture, devices were perfused,

290   fixed, and stained for the endothelial marker CD31, fibrosis marker αSMA, and club cell marker

291   CC10. Representative images of devices are shown in Fig. 3A, controls in Fig S3.
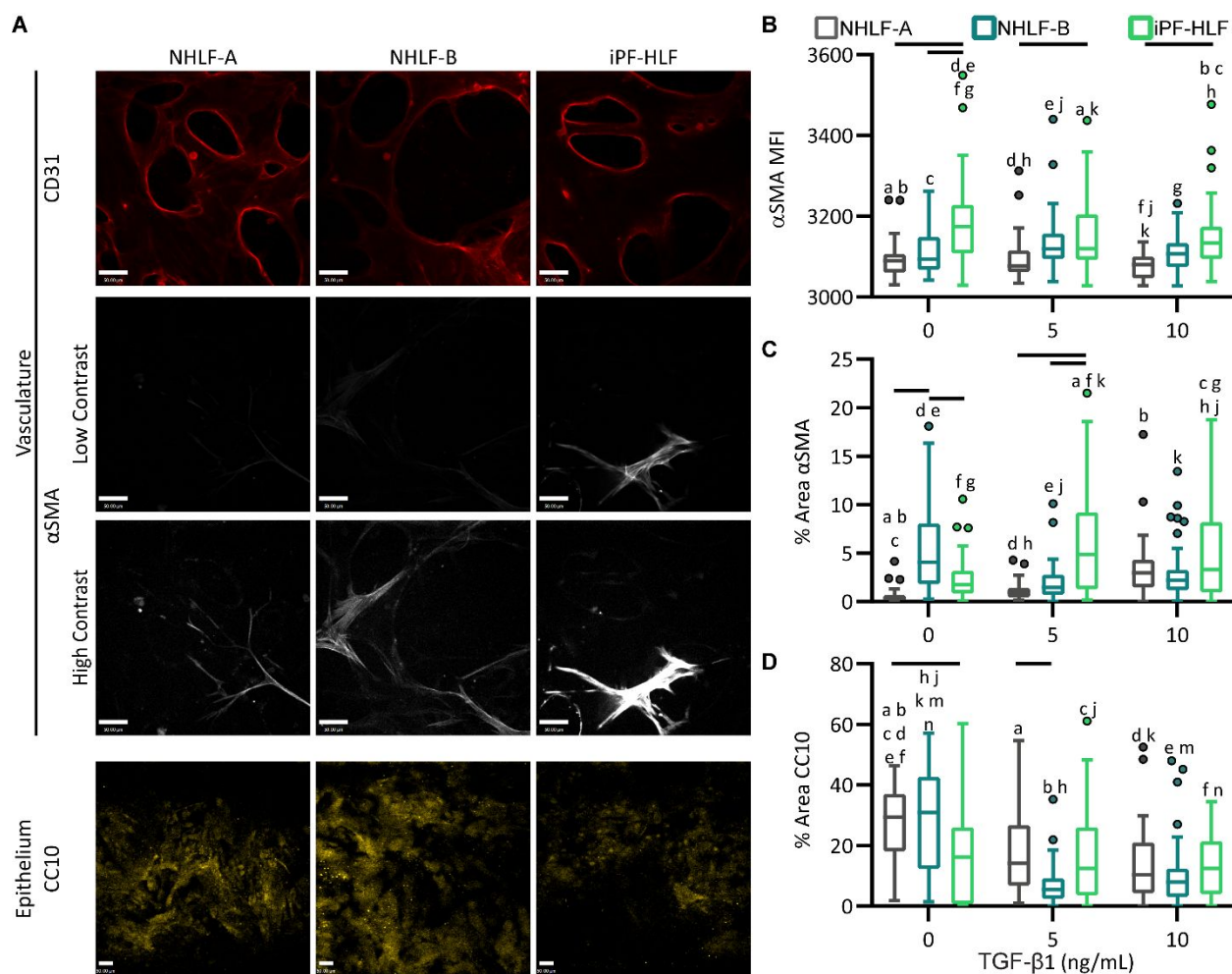
292

293   *Fig. 3. Recapitulation of fibrosis in microphysiological lung-on-a-chip devices.*

294   *Healthy (NHLF from two different donors NHLF-A and -B) and diseased (iPF-HLF) fibroblasts*

295   *were co-cultured with HUVECs below the SAEC epithlium and treated for 3 days with 0, 5, or 10*

296   *ng/mL TGF-β1 to initiate myofibroblast development similar to that in fibrosis. Myofibroblastic*

297   *phenotype was measured using αSMA staining. (A) Representative confocal images with no*

298   *TGF-β1 showing robust vascular network formation (CD31, red) and formation of αSMA*

299   *positive myofibroblasts (white, low and high contrast) as well as formation of airway club cells*

300   *as indicated by CC10 expression (yellow), scale bars = 50 μm; images were linearly contrasted*

301   *for clarity. (B) Mean fluorescence intensity and (C) percent area from confocal images for*

302   *αSMA+ fibroblasts at various TGF concentrations. (D) Percent area of airway epithelium CC10*

303   *staining at various TGF concentrations. n = 20-40 images; two-way ANOVA, bars indicate p <*

304   *0.05 significance within treatment group, letters mark significance across groups.*

305

306   The fluorescence intensity threshold for αSMA was set on isotype controls. Noticeably

307   the αSMA is faint in NHLF-A and NHLF-B and bright in the iPF-HLF which when quantified

308   shows the iPF-HLF devices have a higher mean fluorescence intensity for αSMA across all TGF-

309   β1 treatment groups, Fig. 3C. This suggests that for a fibrosis-like model we can simply switch

310   the co-cultured fibroblasts for diseased donors. With increased TGF-β1, NHLF-A αSMA

311   percentage appears to follow the expected trend with increasing median αSMA area from

312   untreated at 0.3% to 0.9% and 3% for 5 and 10 ng/mL of TGF-β1, respectively, Fig 3C. Oddly,

313   NHLF-B without TGF-β1 treatment had a larger spread and higher median αSMA area of 4.1%

314   than the TGF-β1 treatments with medians at 1.5% and 2.2% respectively. iPF-HLF devices also

315   appeared to increase slightly with TGF-β1 from 1.8% to 4.9% and 3.3% across treatment groups.

316   Although TGF-β1 was able to increase αSMA to create a fibrotic microenvironment, the iPF-

317   HLF had consistently higher expression based on Mean Fluorescence Intensity (MFI). This

318   suggests that we can use either model as a fibrosis-mimicking, microphysiologic pulmonary

319   device.

320 Club cells are immunomodulatory secretory cells within the lung environment that have

321 the potential to differentiate into either type I or II epithelial cells upon injury and have been

322 shown to alter lung function in disease[22,23]. Across both NHLF groups the area of CC10 (club

323 cell marker) expression of the SAECs appears to decrease with the TGF-β1 treatment, Fig. 3D

324 The NHLF-A medians decreased from 29% to 14% and 10%, NHLF-B decreased from 31% to

325 5.4% and 8% for NHLF-B, while iPF-HLF medians were all below 20% (16%, 12% and 12%).

326 The loss of club cell markers and secretions has been implicated as a biomarker for pulmonary

327 disease (e.g. smoking, COPD) progression[23,24]. These results show that this microphysiological

328 device may be used to study the effects of diseased fibroblasts on epithelial phenotypes.

329 Since NHLF-B and iPF-HLF both appear to have higher starting αSMA levels in the

330 untreated group than NHLF-A and were higher than the isotype control (median = 0.2%), we

331 chose these two lots for studies with 100 µg/mL (540 µM) Pirfenidone. Pirfenidone and

332 Nintedanib are currently the only anti-fibrotics available for iPF. While neither drug is able to

333 cure fibrosis, and their effects are patient dependent, they do appear to delay severity[25,26].

334 Although Nintedanib is a potent vasculogenic inhibitor and has been shown to prevent

335 angiogenesis in microvasculature-on-a-chip[27], Pirfenidone was chosen for these studies as it has

336 been shown to reduce αSMA to a greater extent *in vitro* and can be measured by

337 immunofluorescence[19,28,29]. The experimental protocol was similar to the previous fibrosis

338 experiment with devices seeded with NHLF-B or iPF alongside HUVECs, NHLF-A in the outer

339 channel, and SAECs in the airway channel. On Day 6, 10 ng/mL of TGF-β1 was supplemented

340 into the media, and on Day 8, a subset were also treated with 100 µg/mL (540 mM) of

341 Pirfenidone for 24 hours. Devices were stained for CD31 and αSMA to image the vascular

342   compartment and the airway was stained with the epithelial marker Tubb4, representative images

343   of changes in Tubb4 staining can be found in Fig. 4A, controls in Fig. S4.
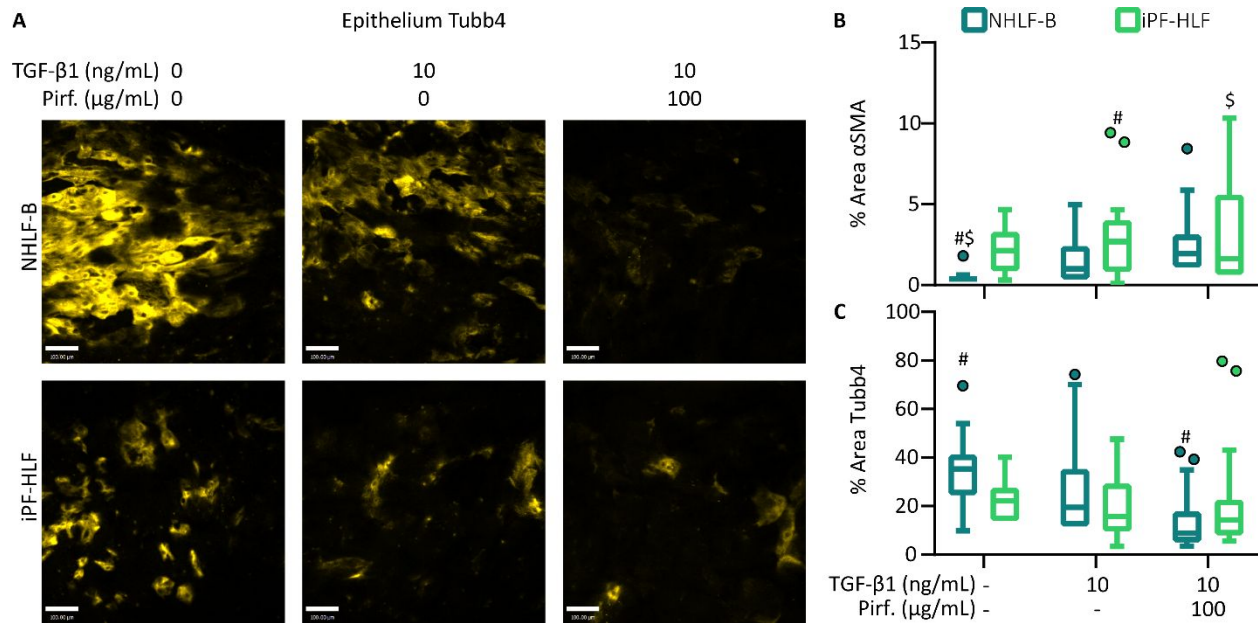
344

345   ***Fig. 4. Pirfenidone fails to reduce TGF-β induced αSMA expression in myofibroblasts***

346   ***in the microphysiologic devices.*** *Devices were seeded with HUVECs, NHLF-B or iPF-HLF in*

347   *the interstitial compartment under the SAEC epithelium and treated with or without 10 ng/ml*

348   *TGF-β ± 100 µg/mL of Pirfenidone (Pirf.). Epithelium were stained with β-tubulin IV (Tubb4) a*

349   *differentiation marker for ciliated cells. (A) Representative images of Tubb4 (yellow) staining in*

350   *the epithelial layer, scale bars = 100 µm; images linearly contrasted for clarity. (B) Percent*

351   *area of αSMA staining does not respond to the Pirfenidone treatment (C) Percent area of Tubb4*

352   *staining appears to decrease with increased TGF-β1. n = 15-20; two-way ANOVA, bars indicate*

353   *p < 0.05 significance within treatment group, symbols mark significance across groups.*

354

355   The αSMA median area for NHLF-B devices increased slightly from 0.4% in the

356   untreated group to 1.0%, and 1.9% for 10 ng/mL or 10 ng/mL TGF-β1 and Pirfenidone

357   treatment, respectively (0.02% for isotype control), Fig. 4B. iPF-HLF median percent αSMA

358   staining were similar to the previous experimental results with medians at 2.1%, 3.7, and 1.6%

359   across treatment groups. The Pirfenidone treatment was unable to attenuate the αSMA

360   expression in these microphysiologic devices.

361   Furthermore, Tubb4, a marker of epithelial differentiation, in these devices also

362   decreased with increased TGF-β1 from 35% untreated to 20%, and 9% in the NHLF-B devices

363   and from 22% to 16%, and 14% across the iPF-HLF groups, Fig. 4C. This shows that, both the

364   TGF-β1 and iPF-HLFs in the co-culture are affecting the development and polarization of the

365   pulmonary epithelium. Interestingly, neither the fibroblasts, nor the epithelial tubulin staining

366   appeared to respond to this Pirfenidone treatment, however, Pirfenidone is often used in high

367   doses (1-2 mM) to reduce pro-fibrotic markers and the dose used in these studies may have been

368   too low to induce any visible changes. Future dose optimization studies over a longer duration

369   alongside donor variability is therefore warranted to investigate the effects of Pirfenidone.

370   Although the two experimental batches of αSMA NHLF-B trends are not identical, the

371   iPF-HLF group had consistently higher median αSMA than the NHLF groups. Additionally, the

372   response from the epithelium suggests that while using αSMA as the primary measure of fibrosis

373   the effect of TGF-β1 and/or incorporation of diseased fibroblasts in the vasculature co-culture

374   affects the development and functionality of the airlifted epithelial airways. This shows that the

375   microphysiologic device allows for the study of epithelial-fibroblast interactions in a more

376   physiologically relevant three-dimensional structure. Without changing the design of the device

377   different co-cultures in the device can be used to create alternative disease models such as

378   cancer, Fig. S5, or cystic fibrosis (CF) with neutrophil migration.

379   Neutrophilic inflammation in the lungs occurs for diseases such as acute respiratory

380   distress syndrome (ARDS), chronic obstructive pulmonary disorder (COPD), iPF, and CF [30–34].

381   However, the 0.4 μm PETE membrane of the device, and widely used in other reported devices,

382   is essentially impermeable to cell migration and larger porous membranes failed to hold an air-

383   liquid interface in these devices. To create a more physiologically relevant membrane, a vitrified

384   collagen thin film was fabricated directly onto the microphysiologic devices as previously

385   described[9]. The human-fibrinogen/collagen mixtures in the central channels appeared to be

386   incompatible with the change in membrane properties, and 100% of devices fully collapsed by

387   Day 5 of culture. Previously published microvascular devices used bovine fibrinogen[5,7], which

388   proved to be successful at a 4 mg/mL fibrinogen to 1 mg/mL collagen hydrogel mixture in this

389   central channel for the length of these cultures.

390   To create a CF-like microvascularized Lung-on-a-Chip the vascular portion of the device

391   was seeded as the previous normal devices: NHLF-B with HUVECs in the central channel and

392   NHLF-A in the outer channels. The airways were then seeded with SAEC or CF human

393   bronchial epithelium (CF HBE). CF is an autosomal recessive disease, and the donor information

394   provided by the manufacturer did not include the specific mutation information. Devices were

395   cultured for 9 days, then CellTracker Deep Red labeled neutrophils were introduced into 1 media

396   port of the vascular layer and 15 μL of PBS, 100 nM Leukotriene B4 (LTB4), or 100 ng/mL

397   lipopolysaccharide (LPS) were added to the airway channels. Both LTB4 and LPS often used in

398   neutrophilic migration assays *in vitro* and *in vivo*; LTB4 is a potent chemotactant produced

399   during inflammation while LPS is an endotoxin often used to induce inflammation. After 3 hours

400   of incubation, the devices were perfused with 70kDa FITC-dextran, Fig. 5A. A single plane of

401   the device microvasculature was imaged as the FITC-dextran (green) perfused the network and

402   showed the neutrophils (white) aligning with these networks. The devices were then repeatedly

403   washed to remove the FITC-dextran, fixed and stained and imaged on a confocal microscope,

404   representative image Fig. 5B.

405
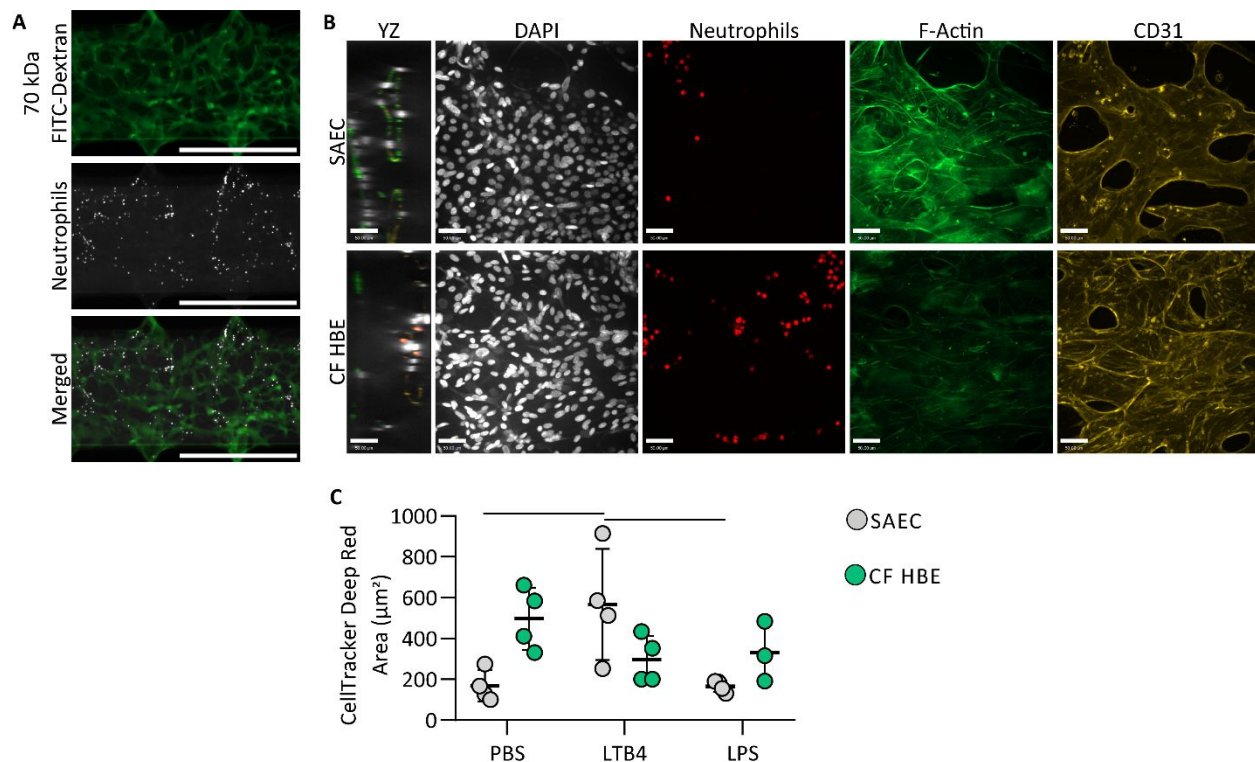
406

407   **Fig. 5. Development of a Cystic Fibrosis (CF) mimicking microphysiological device to**

408   **study effect of CF-like epithelium on neutrophil migration.** *Devices were seeded with a co-*

409   *culture of HUVECs and NHLF-B in the interstitum compartment and with either SAEC or CF*

410   *HBE in the airway compartment. After 9 days of culture, CellTracker Deep Red labeled healthy*

411   *human neutrophils were added to the vasculature media ports and airways were treated with*

412   *PBS, or chemoattractants, LTB4 or LPS to recruit neutrophils into the vascular networks. (A)*

413   *Representative images of perfusable vasculature and CellTracker Deep Red labeled neutrophils,*

414   *showing neutrophils inside the vascular network. scale bars = 1000 μm. (B) Extended focus*

415   *confocal images of representative SAEC and CF HBE PBS treated devices showing neutrophil*

416   *recruitment into the vascular networks. YZ imaging shows vessels below the epithelial layer*

417   *seeded on vitrified collagen, scale bar = 50 μm. (C) Neutrophil recruitment measured by*

418   *CellTracker Deep Red area across the central channel appears higher in the CF-HBE devices*

419   *treated with PBS (p = 0.07), while normal SAECs treated with LTB4 shows increased neutrophil*

420   *chemotaxis compared to the PBS treated group; n = 3-4 devices; two-way ANOVA, bars indicate*

421   *p < 0.05. Images linearly contrasted for clarity.*

422

423   The fluorescent area of the migrated neutrophils across the vasculature appears to be

424   higher in the PBS CF-HBE devices than the SAEC, Fig. 5C, confirming that the device

425   accurately models how CF epithelial cells increase neutrophil migration (p = 0.07) compared to

426   normal epithelial cells. The CF airway epithelium is known to be involved in the innate immune

427   system cytokine secretion and neutrophil recruitment[35].

428   While there was no difference in the area of neutrophils in the CF HBE devices

429   regardless of treatment, the LTB4 treated SAEC devices were significantly higher than the PBS

430   and LPS treated SAEC devices. LTB4 is often a more potent chemoattractant than LPS and thus

431   induced more efficient at neutrophil recruitment at this time frame. These results show the

432   potential for this vascularized Lung-on-a-Chip to be used for studying neutrophilic inflammation

433   in the context of lung disease and regulation of the innate immune system by healthy and

434   diseased lung epithelium.

435

436   **Conclusions**

437   Current microfluidic models of the respiratory airways are similar to transwell-like

438   cultures with monolayers of epithelium and endothelium separated by a thin film[1,36,37]. While this

439   allows for close crosstalk between the epithelium and endothelium it does not allow for a 3D

440   microvascular network or the inclusion of fibroblasts that are critical to fibrosis models.

441   Attempts at creating more advanced pulmonary models took this single channel co-culture

442   approach and integrated an additional layer for a 3-compartment device with a hydrogel layer

443   (with or without fibroblasts) between two monolayer cell cultures[3,4]. While open-top

444   microvasculature devices have been fabricated and provide similar structure, the high porosity

445   and thickness of the membrane create a large physical barrier between the microvasculature and

446   the open compartment[7]. These models allow for the main cellular components to be included;

447   however, they are not in a physiologically relevant structure. Here, we started with a

448   microvascular platform[5,6,10] and integrated a thin film (PETE or vitrified collagen) membrane to

449   grow epithelium at an air-liquid interface to create a microvascularized lung epithelium model

450   with fibroblasts in a more physiologically relevant structure. We then took this device and

451   formatted it into a 96-well plate for higher throughput fabrication and easier handling. We have

452   shown the groundwork for developing a fibrotic lung microenvironment defined by an increase

453   in αSMA positive fibroblasts and shown the influence of the fibroblast disease state on reducing

454   club cell and tubulin staining in healthy epithelium. Additionally, we have shown the

455   microphysiologic device can be used as a platform technology where cell types can be easily

456   exchanged for diseases of interest e.g. cancer or CF and that this microfluidic device can be used

457   to incorporate the innate immune system as other microvascular network models.

458   The readers should be aware of some limitations of this model. Currently the device

459   design does not include the dynamic movement of media in the endothelial compartment as

460   previous single channel designs have used[1,3] nor does this device include the

461   expansion/contraction of the membrane to replicate the cyclic mechanical strain of breathing[37].

462   We have used pooled HUVECs to recreate the vasculature rather than primary human

463   endothelium. Primary lung endothelium's vasculogenesis may be lot-dependent and donor-

464   screening would be needed for successful network formation. In these studies the airlifted

465   interface for the lung epithelium was maintained for 4-8 days; although ALI cultures range from

466   one[38] to two weeks[1], often 4 weeks are needed for full pseudostratified differentiation of

467   bronchial epithelial cells[39]. the main readout for these studies was microscopy, alternative

468   measurements such as Luminex or flow cytometry on transmigrated neutrophils may be limited

469   by the low total number of cells in these co-cultures. In addition, for migration studies it would

470   be important to improve the vitrified collagen membrane to reduce the device failure rates and

471   improve perfusion. Future work should focus on improving this aspect of the device.

472   Despite these limitations, our results suggest that the lung-on-a-chip device described

473   here could have significant impact in studying epithelial-endothelial-fibroblast crosstalk in

474   normal lung models as well as in a variety of inflammatory and interstitial lung disease models,

475   using not only patient-derived primary cells, but also using iPSC-derived cells with our without

476   specific gene-editing to ask certain biological questions. The device could be used as a platform

477   tool for disease modeling and drug screening, for understanding fundamental lung biology, and

478   as a patient-specific personalized medicine tool for understanding or predicting potential

479   treatment effects.

480

References

1. Benam, K. H. *et al.* Small airway-on-a-chip enables analysis of human lung inflammation and drug responses in vitro. *Nat Meth* **13**, 151–157 (2016).

2. Park, J. Y. *et al.* Development of a functional airway-on-a-chip by 3D cell printing. *Biofabrication* **11**, 015002 (2019).

3. Sellgren, K. L., Butala, E. J., Gilmour, B. P., Randell, S. H. & Grego, S. A biomimetic multicellular model of the airways using primary human cells. *Lab Chip* **14**, 3349–3358 (2014).

4. Humayun, M., Chow, C.-W. & Young, E. W. K. Microfluidic lung airway-on-a-chip with arrayable suspended gels for studying epithelial and smooth muscle cell interactions. *Lab Chip* **18**, 1298–1309 (2018).

5. Chen, M. B. *et al.* On-chip human microvasculature assay for visualization and quantification of tumor cell extravasation dynamics. *Nat. Protoc.* **12**, 865–880 (2017).

6. Kim, S., Lee, H., Chung, M. & Jeon, N. L. Engineering of functional, perfusable 3D microvascular networks on a chip. *Lab Chip* **13**, 1489 (2013).

7. Oh, S. *et al.* "Open-top" microfluidic device for in vitro three-dimensional capillary beds. *Lab Chip* **17**, 3405–3414 (2017).

8. Paek, J. *et al.* Microphysiological Engineering of Self-Assembled and Perfusable Microvascular Beds for the Production of Vascularized Three-Dimensional Human Microtissues. *ACS Nano* **13**, 7627–7643 (2019).

9. Mondrinos, M. J., Yi, Y.-S., Wu, N.-K., Ding, X. & Huh, D. Native extracellular matrix-derived semipermeable, optically transparent, and inexpensive membrane inserts for microfluidic cell culture. *Lab Chip* **17**, 3146–3158 (2017).

523   10.   Nelson, M. R. *et al.* A Multi-Niche Microvascularized Human Bone-Marrow-on-a-Chip.

524   *bioRxiv* 2019.12.15.876813 (2019) doi:10.1101/2019.12.15.876813.

525   11.   Phan, D. T. T. *et al.* A vascularized and perfused organ-on-a-chip platform for large-scale

526   drug screening applications. *Lab Chip* **17**, 511–520 (2017).

527   12.   Aran, K., Sasso, L. A., Kamdar, N. & Zahn, J. D. Irreversible, direct bonding of

528   nanoporous polymer membranes to PDMS or glass microdevices. *Lab Chip* **10**, 548

529   (2010).

530   13.   Chuah, Y. J. *et al.* Simple surface engineering of polydimethylsiloxane with

531   polydopamine for stabilized mesenchymal stem cell adhesion and multipotency. *Sci. Rep.*

532   **5**, 18162 (2016).

533   14.   Blundell, C. *et al.* A microphysiological model of the human placental barrier. *Lab Chip*

534   (2016) doi:10.1039/C6LC00259E.

535   15.   Schindelin, J. *et al.* Fiji: an open-source platform for biological-image analysis. *Nat.*

536   *Methods* **9**, 676–682 (2012).

537   16.   Martinez, F. J. *et al.* Idiopathic pulmonary fibrosis. *Nat. Rev. Dis. Prim.* **3**, 17074 (2017).

538   17.   Selman, M. & Pardo, A. Idiopathic pulmonary fibrosis: an epithelial/fibroblastic cross-talk

539   disorder. *Respir. Res.* **3**, 3 (2002).

540   18.   Fernandez, I. E. & Eickelberg, O. The impact of TGF-β on lung fibrosis: From targeting

541   to biomarkers. in *Proceedings of the American Thoracic Society* vol. 9 111–116 (2012).

542   19.   Asmani, M. *et al.* Fibrotic microtissue array to predict anti-fibrosis drug efficacy. *Nat.*

543   *Commun.* **9**, (2018).

544   20.   Tomasek, J. J., Gabbiani, G., Hinz, B., Chaponnier, C. & Brown, R. A. Myofibroblasts

545   and mechano: Regulation of connective tissue remodelling. *Nature Reviews Molecular*

546   *Cell Biology* vol. 3 349–363 (2002).

547   21.   Sucre, J. M. S. *et al.* A 3-Dimensional Human Model of the Fibroblast Activation that

548   Accompanies Bronchopulmonary Dysplasia Identifies Notch-Mediated Pathophysiology.

549   *Am. J. Physiol. Lung Cell. Mol. Physiol.* (2016).

550   22.   Zheng, D. *et al.* Differentiation of Club Cells to Alveolar Epithelial Cells in Vitro. *Sci.*

551   *Rep.* **7**, (2017).

552   23.   Zhai, J. *et al.* Club Cell Secretory Protein Deficiency Leads to Altered Lung Function.

553   *Am. J. Respir. Crit. Care Med.* **199**, 302–312 (2018).

554   24.   Park, H. Y. *et al.* Club cell protein 16 and disease progression in chronic obstructive

555   pulmonary disease. *Am. J. Respir. Crit. Care Med.* **188**, 1413–9 (2013).

556   25.   Noble, P. W. *et al.* Pirfenidone in patients with idiopathic pulmonary fibrosis

557   (CAPACITY): Two randomised trials. *Lancet* **377**, 1760–1769 (2011).

558   26.   Vancheri, C. *et al.* Nintedanib with Add-on Pirfenidone in Idiopathic Pulmonary Fibrosis.

559   Results of the INJOURNEY Trial. *Am. J. Respir. Crit. Care Med.* **197**, 356–363 (2018).

560   27.   Zeinali, S. *et al.* Human microvasculature-on-a chip: anti-neovasculogenic effect of

561   nintedanib in vitro. *Angiogenesis* **21**, 861–871 (2018).

562   28.   Lehtonen, S. T. *et al.* Pirfenidone and nintedanib modulate properties of fibroblasts and

563   myofibroblasts in idiopathic pulmonary fibrosis. *Respir. Res.* **17**, 14 (2016).

564   29.   Jin, J. *et al.* Pirfenidone attenuates lung fibrotic fibroblast responses to transforming

565   growth factor-β1. *Respir. Res.* **20**, 119 (2019).

566   30.   Grommes, J. & Soehnlein, O. Contribution of neutrophils to acute lung injury. *Mol Med*

567   **17**, 293–307 (2011).

568   31.   Weiland, J. E. *et al.* Lung neutrophils in the adult respiratory distress syndrome. *Am. Rev.*

569   *Respir. Dis.* **133**, 218–225 (1986).

570   32. Hoenderdos, K. & Condliffe, A. The Neutrophil in Chronic Obstructive Pulmonary

571   Disease. Too Little, Too Late or Too Much, Too Soon? *Am. J. Respir. Cell Mol. Biol.* **48**,

572   531–539 (2013).

573   33. Hunninghake, G. W., Gadek, J. E., Lawley, T. J. & Crystal, R. G. Mechanisms of

574   neutrophil accumulation in the lungs of patients with idiopathic pulmonary fibrosis. *J.*

575   *Clin. Invest.* **68**, 259–69 (1981).

576   34. Ratjen, F. *et al.* Cystic fibrosis. *Nat. Rev. Dis. Prim.* **1**, 15010 (2015).

577   35. Conese, M., Copreni, E., Di Gioia, S., De Rinaldis, P. & Fumarulo, R. Neutrophil

578   recruitment and airway epithelial cell involvement in chronic cystic fibrosis lung disease.

579   *J. Cyst. Fibros.* **2**, 129–135 (2003).

580   36. Huh, D. *et al.* A human disease model of drug toxicity-induced pulmonary edema in a

581   lung-on-a-chip microdevice. *Sci. Transl. Med.* **4**, 159ra147 (2012).

582   37. Huh, D. *et al.* Reconstituting organ-level lung functions on a chip. *Science.* **328**, 1662–

583   1668 (2010).

584   38. Yonker, L. M. *et al.* Development of a Primary Human Co-Culture Model of Inflamed

585   Airway Mucosa. *Sci. Rep.* **7**, (2017).

586   39. Rayner, R. E., Makena, P., Prasad, G. L. & Cormet-Boyaka, E. Optimization of Normal

587   Human Bronchial Epithelial (NHBE) Cell 3D Cultures for in vitro Lung Model Studies.

588   *Sci. Rep.* **9**, (2019).

589   #

590